INT. J. NUM. METH. HEAT FLUID FLOW, VOL. 4, 561–573 (1994)

NUMERICAL STUDIES OF MIXED RECIRCULATORY FLOW IN ANNULI OF STATIONARY AND ROTATING HORIZONTAL CYLINDERS WITH DIFFERENT RADIUS RATIOS

T. S. LEE

Mechanical and Production Engineering Department, National University of Singapore, Singapore 0511

ABSTRACT

Mixed recirculatory flow in the annuli of stationary and rotating horizontal cylinders were studied numerically. A set of distorted 'false transient' parameters were introduced to speed up the steady state solution of the unsteady vorticity, energy and stream function–vorticity equations. The inner cylinder of the annuli is assumed heated and rotating at Reynolds numbers that exclude the effects of centrifugal acceleration and three-dimensional Taylor vortices. The Prandtl number considered is in the range of 0.01 to 1.0 and Rayleigh number in the range of 10^2 to 10^6. Radius ratios of the cylinders considered are 1.25, 2.5 and 5.0. For a radius ratio of 2.5, inner cylinder rotation in the Reynolds number range of 0 to 1120 was considered. Vertical eccentricities in the range of $\pm 2/3$ were studied for cases of the rotating inner cylinder. Numerical experiments show that the mean Nusselt number increases with Rayleigh number for both cases of concentric and eccentric stationary inner cylinder. At a Prandtl number of order 1.0 with a fixed Rayleigh number, when the inner cylinder is made to rotate, the mean Nusselt number decreases throughout the flow. At lower Prandtl number of the order 0.1 to 0.01, the mean Nusselt number remained fairly constant with respect to the rotational Reynolds number.

KEY WORDS Mixed recirculatory flow Rotating cylinders Cylindrical annuli Concentric and eccentric cylinders Nusselt number Streamlines

NOMENCLATURE

$\hat{g}$	gravitational vector,
L	characteristics length, $L = (R_o - R_i)$,
M, N	mesh sizes,
$\underline{Nu}$	local Nusselt number,
Nu	mean Nusselt number,
∇P	pressure gradient,
Pr	Prandtl number, $Pr = \upsilon/\alpha$,
r	radial coordinate,
R_i, R_o	inner and outer cylinder radii,
RR	radius ratio, $RR = R_o/R_i$,
Ra	Rayleigh number, $Ra = \beta g L^3 T_m/(\alpha\upsilon)$,
Re	rotational Reynolds number of inner cylinder, $Re = R_i\omega L/\nu$,
t, Δt	time and time increment,
T	temperature,
T_i, T_o	temperatures of inner and outer cylinders,
T_R	reference temperature, $T_R = (T_i + T_o)/2$,
T_m	$T_m = (T_i - T_o)/2$,
u	radial velocity,
v	tangential velocity,
α	thermal diffusivity or angular position of the eccentricity vector ε, measured anti-clockwise from the downward vertical of the gravitational vector through the centre of the heated cylinder,
β	thermal coefficient of volumetric expansion,

0961–5539/94/060561–13$2.00

Received June 1993
Revised December 1993

ε eccentricity, i.e. distance between centres of inner and outer cylinders,
ε_h horizontal eccentricity, positive to the right,
ε_v vertical eccentricity, positive upwards,
η dimensionless transformed radial coordinate, $[\eta = (r - r_i)/(r_o - r_i)]$
θ dimensionless temperature, $\theta = (T - T_R)/T_m$,
ϕ angular coordinate of the original solution region measured from the downward vertical through the centre of outer cylinder,
γ angular coordinate of the transformed solution region measured from a reference angle ϕ_c from the vertical through the centre of outer cylinder, i.e. $\gamma = \phi - (\phi_c - \alpha)$,
ν kinematic viscosity,
ρ reference density corresponding to T_R,
ϕ angular coordinate,
ω_i angular velocity of inner rotating cylinder (positive anti-clockwise),
ψ stream function,
ζ vorticity.

INTRODUCTION

Heat transfer and fluid flow processes in enclosed spaces have been extensively studied due to their importance in energy conversion, storage and transmission systems. Concentric and eccentric annular geometries are most commonly encountered in solar collector–receiver system, cooling system in nuclear reactors etc. A comprehensive and extensive review of these works have been collated by Kuehn and Goldstein[1–3] and others[4–10].

For mixed flow in the annulus between concentric or eccentric cylinders in a rotating system, most work were performed for the cases of vertical cylindrical annulus[11,12]. More recently, the effects of recirculation on the natural convection between the annular region in horizontal rotating cylinders have become a topic of interest[13–21]. The applications of these studies include food processing[22,23] and the interest in seeking improved methods for crystallographic perfection in industrial processes[24,25]. Most of the above studies are for air[13–21] with $Pr = 0.7$ or with concentric cylindrical annuli[17–19]. However, other effects of rotation on heat transfer characteristics for low Prandtl number fluids are encountered in high power electric machines with heated shafts, such as a mercury slip ring assembly. This parameter was studied for a concentric case by Huetz[26] for liquid metals and Gardiner and Sabersky[27] for Prandtl numbers of 2.5, 4.5, 6.5. Some studies on the effects of varying Prandtl number on velocity and temperature distribution were conducted by Singh and Rajvanshi[28] with different cylinder eccentricity. A bipolar coordinate system was used. The temperature field was expressed in the form of a perturbation function. Fuseki *et al.*[29] and Prud'homme and Robillard[23] considered mixed convection between concentric horizontal cylinders. The numerical experiments were limited to a range of parameters (specified by $\sigma = Gr/Re^2$) that specifically exclude the appearance of Taylor vortices. Other studies on mixed natural convection in horizontal eccentric annuli includes Ratzel *et al.*[30] and Projahn *et al.*[31].

The present study introduced a set of distorted 'false transient' parameters to the unsteady vorticity, energy and stream function-vorticity equations. This method speeds up the steady state solution for the fluid motion confined between two horizontal isothermal cylinders. The inner cylinder is assumed heated and rotating at a low Reynolds number. The effects of centrifugal acceleration and three-dimensional Taylor vortices are assumed negligible. Radius ratios of the cylinders considered are 1.25, 2.5 and 5.0. For inner cylinder rotating in the Reynolds number range of 0 to 1120, a radius ratio of 2.5 was considered. Vertical eccentricities in the range of $\pm 2/3$ were also studied for cases of the rotating inner cylinder. The Prandtl number considered is in the range of 0.01 to 1.0 and Rayleigh number in the range of 10^2 to 10^6. For the present study, natural convection is driven by vertical temperature gradient and vertical gravity force. The interaction with the effect of high rotational rate of the inner cylinder is expected to lead to complicated three-dimensional flows with Taylor vortices. Hence, the present study purposely limits the calculations to a range of parameters that would exclude this possibility.

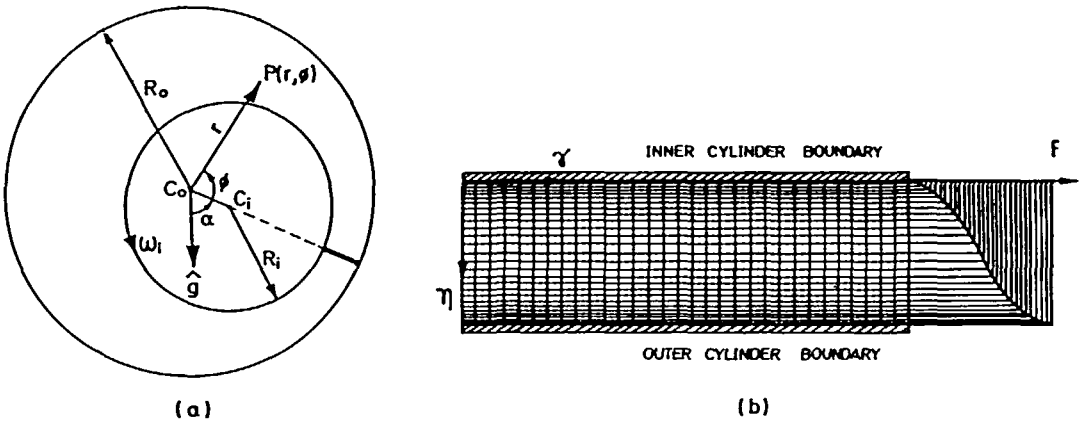

Figure 1 (a) Co-ordinate system in eccentric annular flow region; (b) non-uniform computational mesh in transformed domain

FALSE TRANSIENT SOLUTIONS

A schematic configuration of the eccentric annulus is shown in *Figure 1*. The inner cylinder is assumed heated and rotating. Flow in the annular region is assumed to be two-dimensional, steady and laminar with the absence of Taylor vortices. The detail governing equations which described the above fluid motion of the incompressible fluid between the annulus, subjected to Bousinesq approximation are given in Lee[19,20] and are only briefly presented here:

$$\frac{\partial \theta}{\partial t} + \bar{u}^{*2} \cdot \nabla \theta = \nabla^2 \theta \tag{1}$$

$$\frac{\partial \bar{\zeta}^*}{\partial t} - \nabla \times (\bar{u}^* \times \bar{\zeta}^*) = -RaPr(\nabla \times \theta \hat{g}) + Pr(\nabla^2 \bar{\zeta}^*) \tag{2}$$

$$\bar{\zeta}^* = -\nabla^2 \bar{\psi}^* \tag{3}$$

$$\bar{u}^* = \nabla \times \bar{\psi}^* \tag{4}$$

where the dimensionless variables are: $r^* = r/L$, $t^* = t/(L^2/\alpha)$, $u^* = u/(\alpha/L)$, $v^* = v/(\alpha/L)$, $\zeta^* = \zeta/(\alpha/L^2)$, $\psi^* = \psi/\alpha$ and $\theta = (T - T_R)/T_m$. $r^*, t^*, u^*, v^*, \psi^*$ and θ represent the dimensionless radial coordinate, time, radial velocity, tangential velocity, stream function and temperature respectively. (From hereon, the * representing dimensionless quantities are dropped for simplicity.)

Steady state solution of (1), (2) and (3) may be obtained by some iterative procedure, such as the Jacobi iteration, or by some relaxation methods[32]. If this approach is used, then for each overall iteration loop of the set of steady state equations ($\partial/\partial t = 0$), there will be as many inner iteration loops as there are equations. Each of these inner iteration loops has to converge before the next overall iteration loop can be performed. For the set of steady state form of (1), (2) and (3), this procedure can become very time-consuming. An improved method is to approach the steady state solution through the corresponding unsteady equations. This time-dependent transient approach to the steady state solution is attractive. If there is more than one equation of the vorticity-transport type, then most of the inner iteration loops are eliminated. Unfortunately, (3) remains elliptic in form. Its numerical solution requires an iterative technique at each time step to determine the stress function at that time. The overall solution process is then multi-iterative.

For problems considered here, we are only interested in the steady state solutions. The inner iteration loop of stream function–vorticity equation $\bar{\zeta} = -\nabla^2\bar{\psi}$ seems an unnecessary burden in terms of computing effort. If the steady state solution is unique, and is independent of the transient approach to it, then the steady stage solution of (1)–(3) can be reached by introducing a transient term into the stream function–vorticity equation and treating the stream function as a transport quantity,

$$\frac{\partial\bar{\psi}}{\partial t} = \nabla^2\bar{\psi} + \bar{\zeta} \tag{5}$$

Numerical experimentation shows that the stability characteristics of (1), (2) and (4) varied according to the relatively magnitudes of the source term in the respective equations, and also convective stability of the flow does not effect (5). In terms of numerical stability with a fixed time increment Δt, and fixed mesh sizes, (5) was found to be the most stable, and the vorticity transport equation (2) is numerically most unstable. Hence, some 'false transient' terms are introduced into (5) to 'speed up' the solution and into (2) to stabilize the solution for a fixed time increment. The steady state solution is finally obtained through a set of 'fast and stable' transient equations:

$$\frac{1}{\alpha_\psi}\frac{\partial\bar{\psi}}{\partial t} = \nabla^2\bar{\psi} + \bar{\zeta} \tag{6}$$

$$\frac{1}{\alpha_\xi}\frac{\partial\bar{\xi}}{\partial t} - \nabla\times(\bar{u}\times\bar{\zeta}) = -RaPr(\nabla\times\theta\hat{g}) + Pr(\nabla^2\bar{\zeta}) \tag{7}$$

Through a series of numerical experiments, the optimum values of α_ψ and α_ζ for the fastest convergent rate can be found for the class of fluid flow considered here. As shown in *Figures 2a* and *2b*, the optimum value of α_ψ lies between 1.0 and 10, and the optimum value of α_ζ lies between 0 and 1.0. The time-step used in the numerical solution follow the Courant–Ferderic–Lewis conditions.

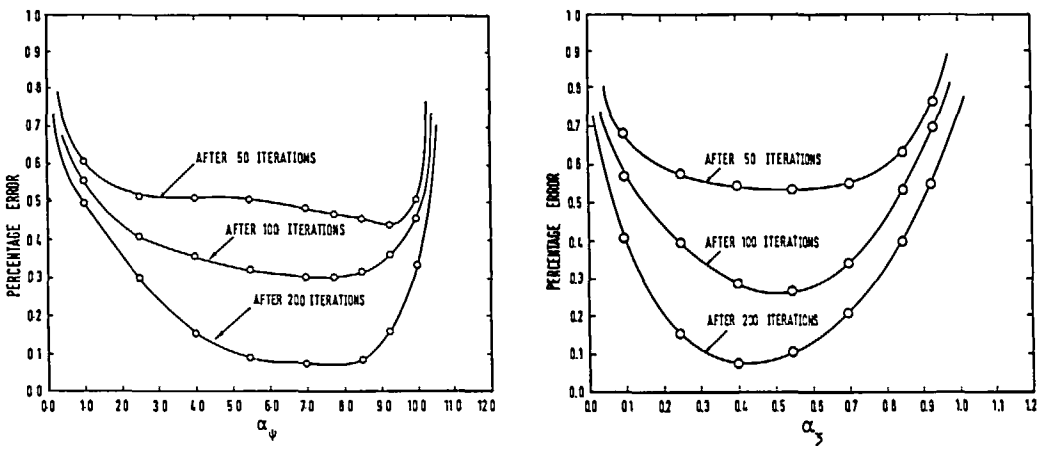

Figure 2 False transient parameters: (a) α_ψ; (b) α_ζ

BOUNDARY CONDITIONS

At the boundaries ψ is constant as there is no flow across the boundaries, i.e.,

$$\left.\begin{aligned}\psi(\eta = 1) &= \psi_o = 0\\ \psi(\eta = 0) &= \psi_i = f(Re)\end{aligned}\right\} \tag{8}$$

where $f(Re)$ is determined by the requirement that the pressure distribution be single-valued.

The stream function ψ_o on the outer cylinder wall is arbitrarily set to zero. For stationary inner cylinder, the stream-function ψ_i on the inner cylinder wall is set equal to the outer cylinder streamline value. This is because the rising plume touches the outer cylinder wall and the net circulating volumetric flow rate around the cylinders is zero when the inner cylinder is not rotating. When the inner cylinder is made to rotate, the streamline value at the inner rotating cylinder wall, ψ_i cannot be pre-assigned. The use of $\partial\psi/\partial n =$ wall velocity, gives solution for which $\partial\psi/\partial s \neq 0$ along the wall of the inner cylinder. This implies that fluid was numerically 'leaked' through the moving inner cylinder wall. In the present study, ψ_i is determined using the criterion that the pressure distribution in the solution region is a single-valued function. Mathematically, this criterion implies that the line integral of the pressure gradient $\partial P/\partial s$ along any closed loop circumscribing the inner cylinder is zero, i.e. $\oint(\partial P/\partial s)\,ds = 0$. $(\partial P/\partial s)$ can be evaluated from the momentum conservation equations.

With the inner cylinder rotating at an angular velocity ω corresponding to a rotational Reynolds number of $Re = R_i\omega L/v$ and assuming no slip at the boundaries, the velocity boundary conditions are:

$$\left.\begin{aligned}u(\eta = 0) &= 0\\ u(\eta = 1) &= 0\\ v(\eta = 0) &= RePr\\ v(\eta = 1) &= 0\end{aligned}\right\} \tag{9}$$

θ at the boundaries is given by:

$$\left.\begin{aligned}\theta(\eta = 0) &= 1\\ \theta(\eta = 1) &= -1\end{aligned}\right\} \tag{10}$$

At the inner and outer boundaries, $\psi =$ constant, hence

$$\zeta = -\beta^2\frac{\partial^2\psi}{\partial\eta^2} + \frac{v}{r} \tag{11}$$

NUMERICAL METHODS

Figure 1a shows the coordinate system of the annulus with an eccentricity $C_iC_o = \varepsilon$ at angle α to the vertical axis. The transformed solution region $(0 \geqslant \eta \leqslant 1,\ 0 \leqslant \gamma \leqslant 2\pi)$ is shown in *Figure 1b*. The lines with constant η in the transformed solution region corresponds to eccentric circles in the original solution region of *Figure 1a*. In the transformed solution region (η, γ) is defined as:

$$\left.\begin{aligned}\eta &= \frac{r - r_i}{r_o - r_i} = f(r, \phi)\\ \gamma &= (\gamma_{ref} - \alpha) + \phi\end{aligned}\right\} \tag{12}$$

with $(\varepsilon + R_i) < R_o$ and $\varepsilon < R_i$,

$$r_o = R_o$$
$$r_i = \varepsilon \cos(\phi) + \{[\varepsilon \cos(\phi)]^2 + (R_i^2 - \varepsilon^2)\}^{1/2}$$

The solution region in *Figure 1a* is 'cut' along the $\gamma = \gamma_{ref}$ radial line and stretched into a rectangular γ–η domain as defined by (8) and shown in *Figure 1b*. In order to obtain better resolution of the solution near the wall regions while preserving the second order accuracy of the finite difference scheme, the continuous rectangular domain is then overlaid with a non-uniform finite difference mesh generator given by:

$$F = \frac{2}{\pi} \sin^{-1}(\eta^{1/2}) \tag{13}$$

At the node points, the finite difference solutions to (1), (4), (6) and (7), with their boundary conditions are obtained. The numerical procedure used involves an alternating direction implicit (ADI) method originally proposed by Peaceman and Rachford[37] and is modified here by the inclusion of a weighted time-step factor, σ and the false transient parameter α_ζ. For the vorticity transport equation, the advancement over one time step is accomplished through:

$$\begin{aligned} [I - \sigma\alpha_\zeta \Delta t A_\gamma](\zeta)^* &= [A_\gamma + A_\eta](\zeta)^n + (S_D)^n \\ [I - \sigma\alpha_\zeta \Delta t A_\eta](\zeta)^{**} &= (\zeta)^* \\ (\zeta)^{n+1} &= (\zeta)^n + \Delta t(\zeta)^{**} \end{aligned} \tag{14}$$

where $(\zeta)^*$ and $(\zeta)^{**}$ are dummy variables; A_γ and A_η are matrix operators formed through finite differencing of the governing equations in the γ and η directions respectively; $(S_D)^n$ is the source term evaluated at the most recent solution field; I is an identity matrix. For $\sigma = 1/2$, the above scheme corresponds to the Crank–Nicholson equation.

The same method is adopted in solving the temperature and stream function–vorticity equations. All spatial derivatives are approximated by second-order-accurate central differences. The convective terms in (1) and (7) are approximated by using a second-order up-wind differencing method. The mixed spatial derivatives resulting from the mesh transformation are handled by the method proposed by McKee and Mitchell[34]. The resulting linear set of finite difference equations is then solved by an algorithm due to Thomas (see Roach[32]). Three-point backward and forward difference formula are used for derivatives at the boundaries.

Heat transfer at the inner cylinder wall is defined by the mean Nusselt number:

$$\overline{Nu} = \int_0^{2\pi} \left(-\frac{\partial\theta}{\partial r}\right) d\gamma/2\pi \tag{15}$$

The mean Nusselt number is also used as the quantity to indicate steady state convergence. The mean Nusselt number is computed at every twentieth iteration. The steady state criteria is said to have satisfied when a difference of less than 0.1% of a reference Nusselt number $[Nu_{ref} = 1.0]$ is detected. The computation of the Nusselt number requires the differentiation of the temperature function, and should therefore converge at a lower rate than the latter. This has proven satisfactory. The stream function, velocity, temperature and vorticity fields are noted to be steady when the Nusselt number is steady.

RESULTS AND DISCUSSION

The discussion here is based on the steady state results obtained from the false transient solutions of the governing equations with initial values of ψ, u, v, θ, and ζ all set to zero, except the temperature at the inner and outer cylinder walls. The temperature is $+1$ at the inner wall and

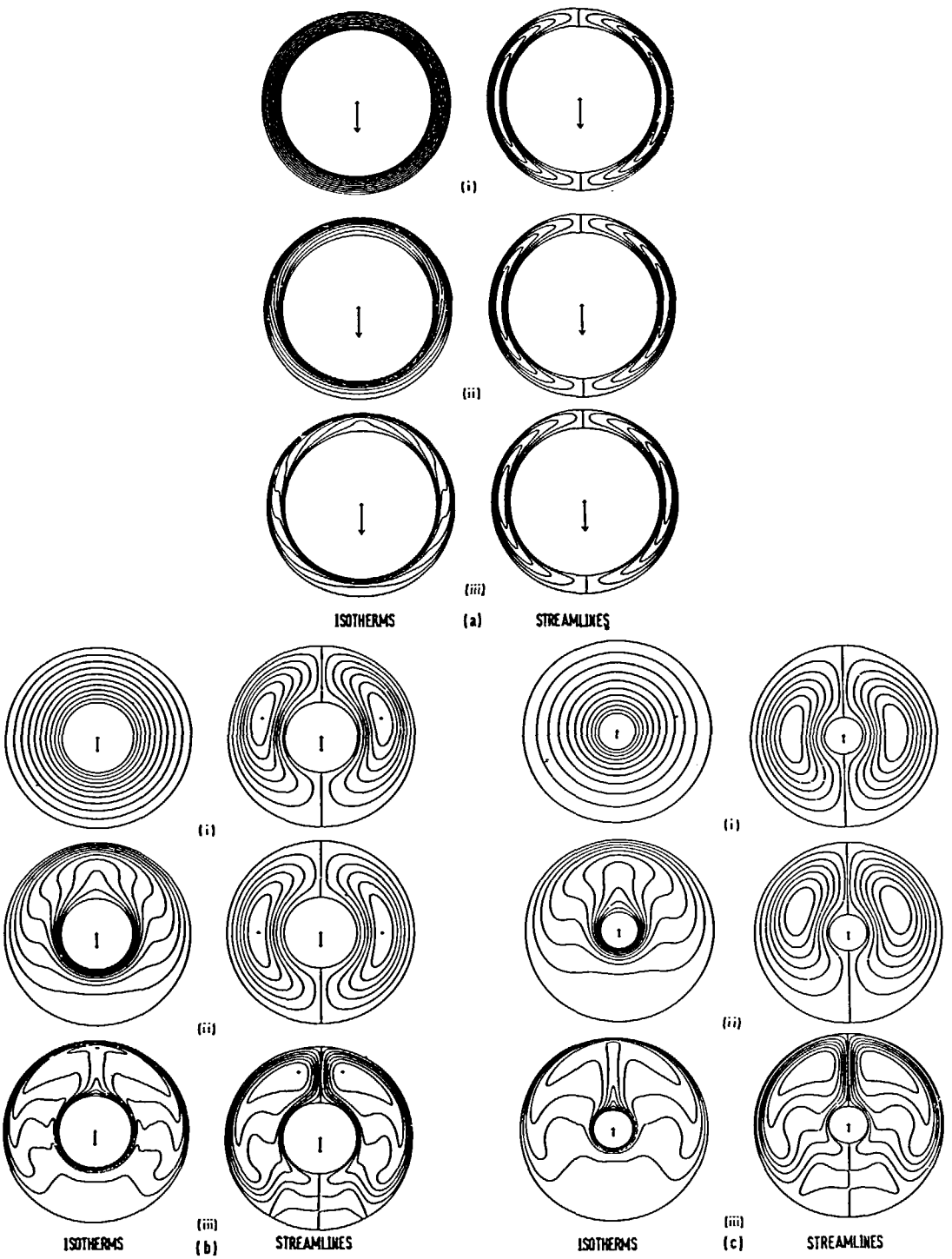

Figure 3 Stationary cylinders ($Re = 0$, $Pr = 1.0$): streamlines and isotherms. (a) $RR = 1.25$: (i) $Ra = 10^2$, (ii) $Ra = 10^4$, (iii) $Ra = 10^6$. (b) $RR = 2.5$: (i) $Ra = 10^2$, (ii) $Ra = 10^4$, (iii) $Ra = 10^6$. (c) $RR = 5.0$: (i) $Ra = 10^2$, (ii) $Ra = 10^4$, (iii) $Ra = 10^6$

-1 at the outer wall. The solutions were initially tested with time steps of 0.1, 0.01, 0.001 and 0.0001 and mesh sizes of 21×41, 41×81, 81×161 and 161×321. It was found that the variations of the solution fields were not significant (of the order of 0.1% in the temperature field, 0.1% in the streamline field, 0.2% in the vorticity field and 0.1% in the mean Nusselt number obtained) between time step of 0.001 and 0.0001, and mesh sizes of 81×161 and 161×321. Hence, for the results obtained here, a dimensionless time increment of 0.001 and mesh size of 81×161 were used.

With the above time step and mesh size, the model was initially computed for stationary cylinders of concentric configurations with $Pr \cong 1.0$ (air) where information on streamline patterns and isotherm contours from other investigators are readily available for comparison. *Figures 3a–3c* show the effects of Ra on the streamlines and isotherms for concentric annulus of different radius ratios of $RR = 1.25$, 2.5 and 5.0. It is seen that when Ra is less than 10^3 [*Figures 3a(i)*, *3b(i)* and *3c(i)*], the isotherms are almost concentric circles, resembling those of pure conduction. The counter rotating pair of kidney shaped vortices are, however, already quite distinct. These low Ra flows were called 'pseudo-conductive' by Grigull and Hauf[35]. The mean Nusselt number is close to one in this low Ra region. As the Ra is increased further, the increased buoyancy effect causes the fluid to move rapidly. At a Ra of about 10^4 [*Figures 3a(ii)*, *3b(ii)* and *3c(ii)*], the isotherms lost their circular shape. Above this Ra [*Figures 3a(iii)*, *3b(iii)* and *3c(iii)*], a temperature inversion takes place and separate thermal boundary layers are formed on the outer and inner cylinders. At this stage, a thermal plume begins to form at the top of the inner cylinder. For Ra above 10^6, the flow tends to become unstable. It is expected that the flow is turbulent and the validity of the results obtained becomes poor. Interferometric

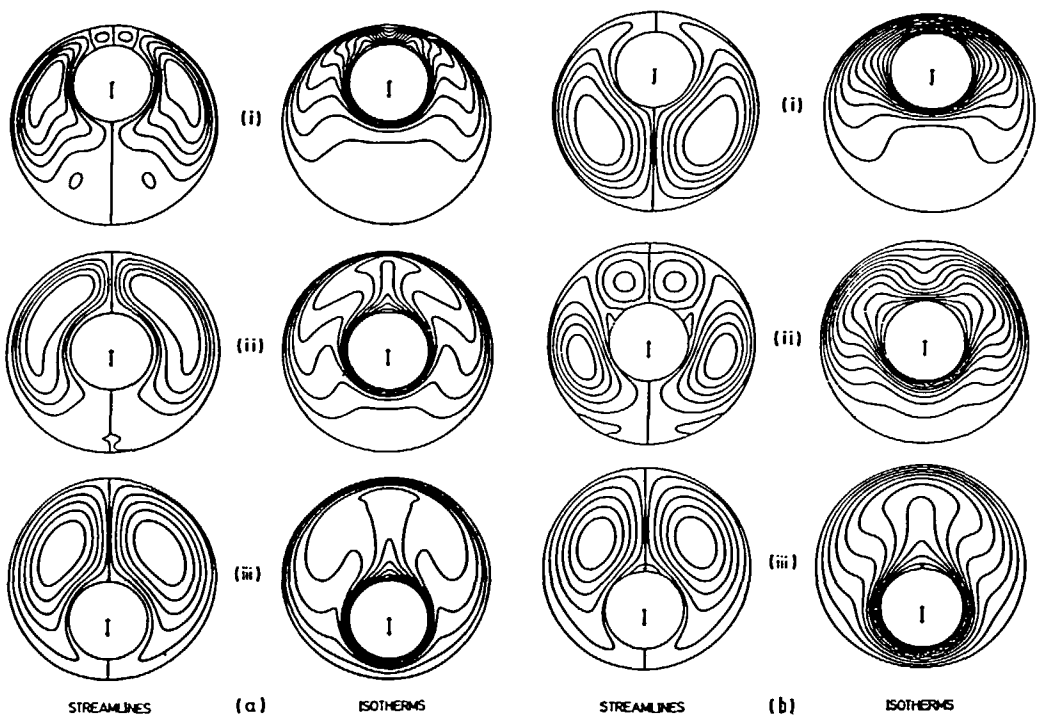

Figure 4 Stationary cylinders ($RR = 2.5$, $Re = 0$, $Ra = 10^5$): streamlines and isotherms. (a) $Pr = 1.0$: (i) $\varepsilon_v = 2/3$, (ii) $\varepsilon_v = 0$, (iii) $\varepsilon_v = 2/3$. (b) $Pr = 0.01$: (i) $\varepsilon_v = 2/3$, (ii) $\varepsilon_v = 0$, (iii) $\varepsilon_v = 2/3$

photographs of Kuehn and Goldstein[3] for $Ra < 10^6$ are similar to the numerical solutions of isotherms and streamlines obtained in this study.

Figure 4 shows the effects of vertical eccentricity on the flow and temperature distributions for $Ra = 10^5$ and $Pr = 1.0$, 0.01 for $RR = 2.5$, $Re = 0$ at vertical eccentricities of $\varepsilon_v = 2/3$, 0, $-2/3$. The immediate effect of displacing the inner cylinder downward is to increase the convective region above the inner cylinder. *Figure 4a* shows that, for $Pr = 1.0$, the single thermal plume above the inner cylinder is enhanced when the inner cylinder is displaced downward. For Prandtl number of 0.01, the bi-thermal plumes observed at some vertical eccentric locations are eliminated when the inner cylinder is displaced downwards [*Figure 4b(ii)–4(iii)*]. Further numerical experiments show that if the Rayleigh number is small ($Ra \leqslant 10^3$), no convective motion can take place for any value of Prandtl number. The mean Nusselt number and the isotherms plot resembles that of pure conduction. The isotherms form concentric circles surrounding the inner cylinder. As the Rayleigh number increases, the convective strength increases. When the convective flow becomes strong enough, temperature inversion begins to take place and the basic counter rotating pair of crescent-shape-like cells will be modified. The extent and the manner in which the modifications on the basic flow patterns take place depend very much on the Rayleigh number, Prandtl number, radius ratio, as well as the eccentricities of the inner cylinder.

The validity of the above numerical results was verified for stationary concentric cylinders[19–21]. Numerical results of Ra vs $\overline{Nu}$ at radius ratios of 1.25, 2.6 and 5.0 for stationary cylinders are shown in *Figure 5*. Converted experimental data of Kuehn and Golstein[1,2] for $RR = 2.6$ are also shown. The correlation curves of Raithby and Holland[36] for $RR = 2.6$ and 1.25, the numerical results of Yang *et al.*[24,25] for $RR = 1.4$ and 2.6, and Projahn *et al.*[31] for $RR = 2.6$ are also plotted on the same figure. The computed results indicate very good agreement with

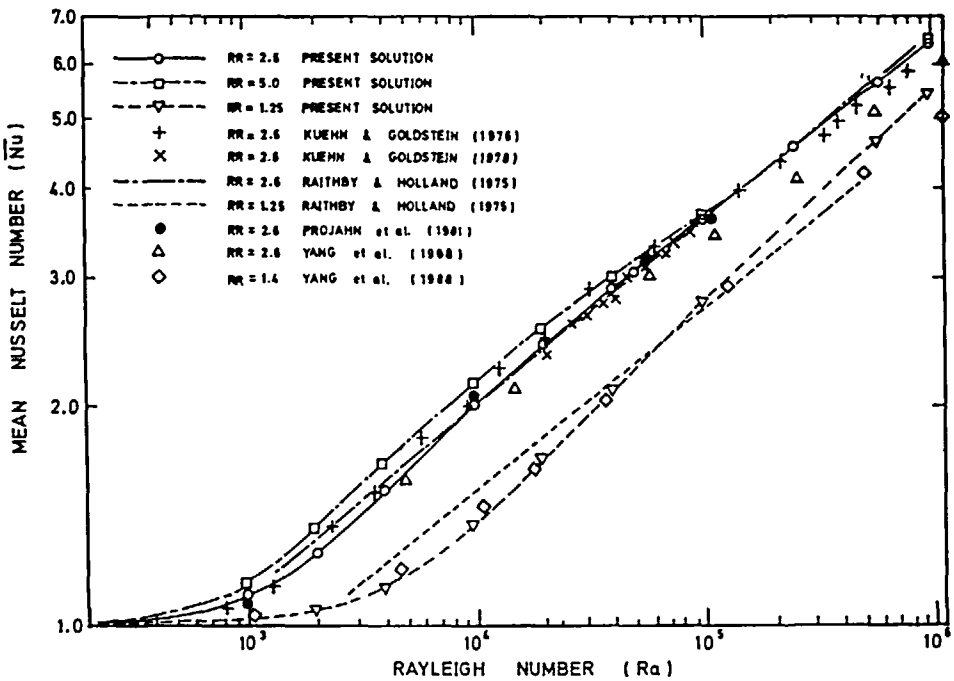

Figure 5 Mean Nusselt number *versus* Rayleigh number at various RR (eccentricity, $\varepsilon = 0.0$)

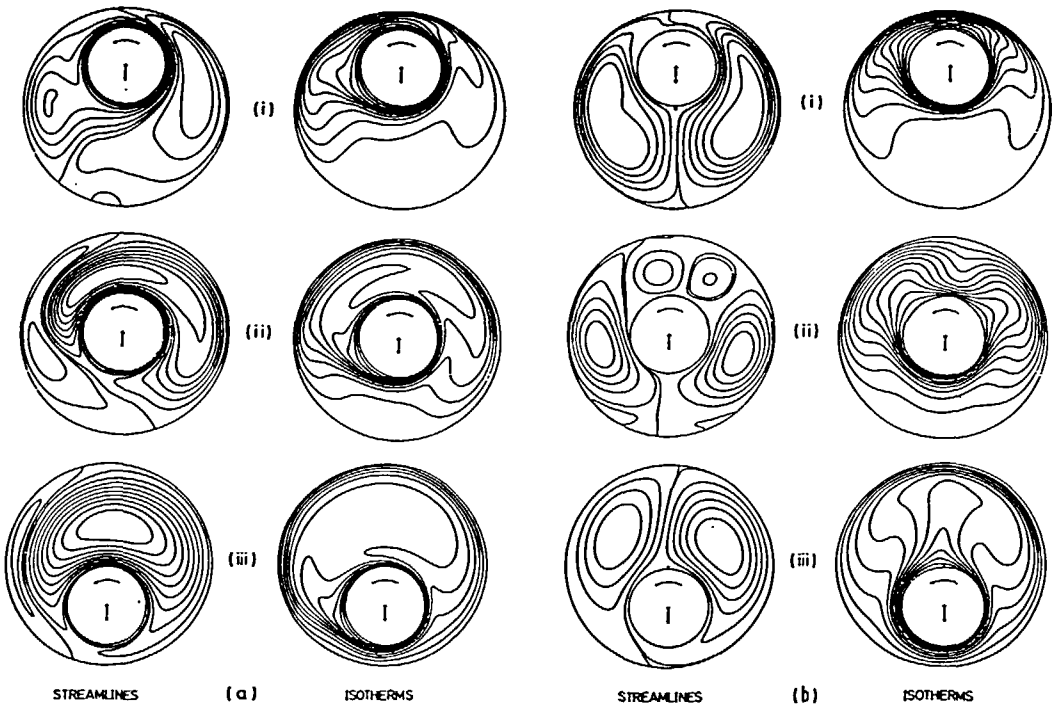

Figure 6 Rotating cylinder ($RR = 2.5$, $Re = 560$, $Ra = 10^5$): streamlines and isotherms. (a) $Pr = 1.0$: (i) $\varepsilon_v = 2/3$, (ii) $\varepsilon_v = 0$, (iii) $\varepsilon_v = -2/3$. (b) $Pr = 0.01$: (i) $\varepsilon_v = 2/3$, (ii) $\varepsilon_v = 0$, (iii) $\varepsilon_v = -2/3$

the published results of other investigators for stationary cylinders. For rotating inner cylinder, no suitable results are available for comparison.

When the inner cylinder is made to rotate, the corresponding streamlines and isotherms are shown in *Figure 6*. A general trend is observed. With the inner cylinder rotating in the counter clockwise direction, any cell on the right of the inner cylinder will be dragged upwards by virtue of the viscous drag. At the same time, any cell on the left of the inner cylinder is being dragged downward by the viscous action of the inner cylinder rotation. The isotherms, as a result, are tilted in the direction of rotation from its corresponding stationary cases. The degree of destruction of the left-hand cell and the enhancement of the right-hand cell depends greatly on the basic flow for a corresponding case of stationary cylinders. For a given Rayleigh number, the general effects of the tilting of thermal plume in the direction of rotation is more pronounced at higher Prandtl number. At higher rotational Reynolds number, the convective strength as compared with the induced viscous drag by virtue of rotation is negligible. The immediate effect of rotating the inner cylinder is to set up a couette-like rotation where all the fluid within the same annular spaces are rotating with virtually the same speed. These couette-like flows are in the form of concentric circles surrounding the inner cylinder. The thermal plume tends to diffuse and the isotherms form circular rings surrounding the inner cylinder suggesting that the mode of heat transfer is conduction dominant.

For low Prandtl number fluid flow (such as mercury with Pr in the order of 0.01), symmetrical bithermal plume was observed above the inner cylinder at certain eccentricities (*Figure 7a*). The flow pattern in the annulus is observed to be multicellular in these cases. The heat transfer characteristics for these fluid flow with low Prandtl number were found to have points of maximum and minimum at the interior nodes, instead of the top and bottom nodes which is

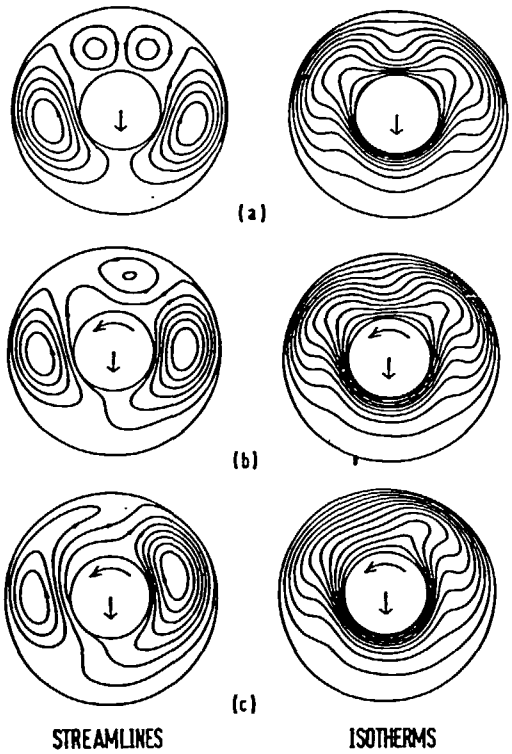

Figure 7 Rotating inner cylinder ($RR = 2.5$, $Pr = 0.02$, $Ra = 10^5$): (a) $Re = 0$, (b) $Re = 560$, (c) $Re = 1120$

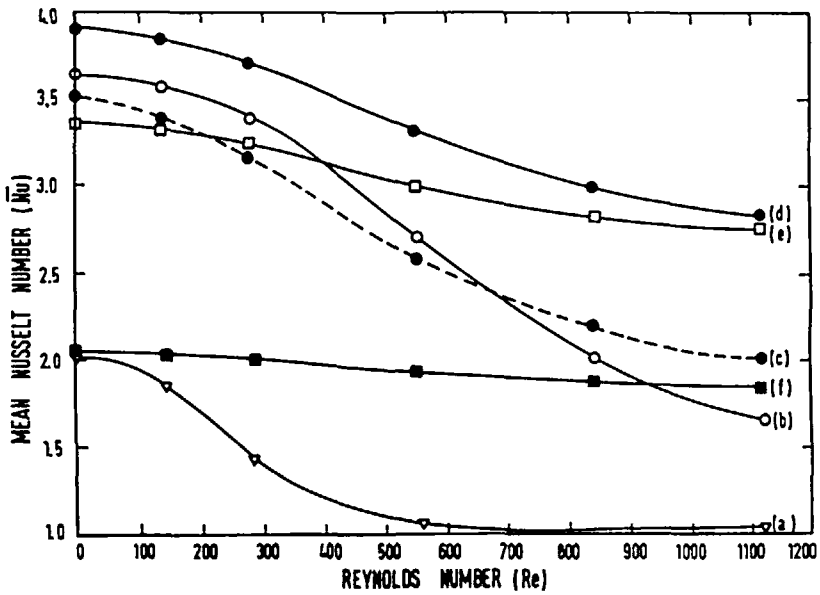

Figure 8 Effects of inner cylinder rotation on $\overline{Nu}$. (a) $\varepsilon_v = 0$: $RR = 2.5$, $Pr = 1.0$, $Ra = 10^4$; (b) $\varepsilon_v = 0$: $RR = 2.5$, $Pr = 1.0$, $Ra = 10^5$; (c) $\varepsilon_v = 2/3$: $RR = 2.5$, $Pr = 1.0$, $Ra = 10^5$; (d) $\varepsilon_v = -2/3$: $RR = 2.5$, $Pr = 1.0$, $Ra = 10^5$; (e) $\varepsilon_v = 0$: $RR = 2.5$, $Pr = 0.1$, $Ra = 10^5$; (f) $\varepsilon_v = 0$: $RR = 2.5$, $Pr = 0.01$, $Ra = 10^5$

known for the high Prandtl number fluids. When the inner cylinder is made to rotate, the flow pattern becomes more complex [*Figures 7b–7c*]. The multicellular flow with its bithermal plume on one side of the annulus for low Prandtl number fluid is suppressed. The net effect is that a single thermal plume is observed to move in the direction opposite to that of the inner rotating cylinder. This thermal plume movement is different and opposite to that observed for the high Prandtl number fluid flow where the monothermal plume on top of the inner cylinder moves in the same direction as the rotation of the inner cylinder.

The corresponding effect of increasing *Re* of the inner cylinder rotation on mean Nusselt number with varying Rayleigh number and Prandtl number is shown in *Figure 8*. At higher Prandtl number [*Figures 8a–8b*], the mean Nusselt number falls with increasing rotational speed of the inner cylinder. The drop in the mean Nusselt number can also be visualized with the aid of the streamline and temperature contours in the numerical experimentations. As the rotational *Re* increases, the convective thermal plume movement above the inner cylinder gradually diminished. Isotherms near the inner cylinder formed into concentric rings with increased isotherm spacings. These isotherm patterns indicate a drop in temperature gradient and hence a drop in mean Nusselt number. When eccentricity is introduced [*Figures 8c–8d*], the mean Nusselt number falls off from its stationary value with increasing rotational Reynolds number in a manner similar to the behaviour of the concentric case. For the case of lower Prandtl number of 0.1 and 0.01, numerical experiments show that the variation of the mean Nusselt number is negligible when the Reynolds number is increased for low *Pr* [*Figures8e–8f*] at fixed *Ra*.

CONCLUSIONS

Mixed recirculatory fluid motion and heat transfer in the annular space between two horizontal cylinders when the inner cylinder is heated has been studied numerically. The cylinders radius ratios considered are 1.25, 2.5 and 5.0. The mean Nusselt number characteristics are obtained for Rayleigh number up to 10^6; Prandtl number in the range of 0.01 to 1.0; and rotational Reynolds number for the inner cylinder up to 10^3. For the range of parameters considered above, numerical experiments show that the mean Nusselt number increases with Rayleigh number for both the cases of concentric and eccentric stationary inner cylinder. At a Prandtl number of order 1.0 with a fixed Rayleigh number, when the inner cylinder is made to rotate, the mean Nusselt number decreases throughout the flow. The flow pattern observed in this study varies significantly with respect to the rotational Reynolds number for lower Prandtl number fluids of the order 0.1 yo 0.01. The mean Nusselt number, however, remained fairly constant with respect to the rotational Reynolds number of the inner cylinder for low Prandtl number fluids.

ACKNOWLEDGEMENTS

The author gratefully acknowledges the financial support of a National University of Singapore Research Grant (No. RP890633) and the assistance of S. Y. Lim and C. L. Soh during the course of this work.

REFERENCES

1 Kuehn, T. H. and Goldstein, R. J. An experimental and theoretical study of natural convection in the annulus between horizontal concentric cylinders, *J. Fluid Mech.*, **74**, 695–719 (1976)
2 Kuehn, T. H. and Goldstein, R. J. An experimental study of natural convection heat transfer in concentric and eccentric horizontal cylindrical annuli, *ASME J. Heat Transfer*, **100**, 635–640 (1978)
3 Kuehn, T. H. and Goldstein, R. J. A parametric study of Prandtl number and diameter ratio effects on natural convection heat transfer in horizontal cylinder annuli, *ASME J. Heat Transfer*, **102**, 768–770 (1980)
4 Pepper, D. W. and Cooper, X. X. Numerical solution of natural convection in eccentric annuli, *AIAA/ASME 3rd Joint Thermophys., Fluids, Plasma Heat Transfer Cojf., St. Louis*, AIAA Paper No. 82-0983 (1980)

5 Babus'Haq, R. F., Probert, S. D. and Shilston, M. J. Natural convection across cavities: design advice, *Appl. Energy*, **20**, 161–188 (1985)
6 Hessami, M. A., Pollard, A., Powe, R. D. and Ruth, D. W. A study of free convective heat transfer in a horizontal annulus with large radii ratio, *J. Heat Transfer*, **107**, 603–610 (1985)
7 Glakpe, E. K., Watkins, C. B. and Cannon, J. N. Constant heat flux solutions for natural convection between concentric and eccentric horizontal cylinders, *Num. Heat Transfer*, **10**, 279–295 (1986)
8 Bishop, E. H. and Brandon, S. C. Heat transfer by natural convection of gases between horizontal isothermal concentric cylinders: the expansion number effect, *ASME-JSME Thermal Eng. Joint Conf.*, Vol. 2, pp. 275–280 (1987)
9 Bishop, E. H. Heat transfer by natural convection of helium between horizontal isothermal concentric cylinders at cryogenic temperatures, *J. Heat Transfer*, **110**, 109–115 (1988)
10 Castrejon, A. and Spalding, D. B. An experimental and theoretical study of transient free-convection flow between horizontal concentric cylinders, *Int. J. Heat Mass Transfer*, **31**, 273–284 (1988)
11 Hessami, M. A., De Vahl Davis, G., Lenonardi, E. and Reizes, J. A. Mixed convection in vertical cylindrical annuli, *Int. J. Heat Mass Transfer*, **30**, 151–161 (1987)
12 Randriamampiania, ?. ?., Bontoux, A. P. and Roux, B. Boundary driven flows in rotating cylindrical annulus, *Int. J. Heat Mass Transfer*, **30**, 1275–1286 (1987)
13 Lee, T. S. Free and forced convection in concentric and eccentric horizontal cylindrical annuli, *Proc. ASME/JSME Thermal Eng. Joint Conf., Honolulu*, Vol. 3, pp. 125–131 (1983)
14 Lee, T. S. Numerical experiments with laminar fluid convection between concentric and eccentric heated rotating cylinders, *Num. Heat Transfer*, **7**, 77–87 (1984)
15 Lee, T. S., Wijeysundera, N. E. and Yeo, K. S. Free convection fluid motion and heat transfer in horizontal concentric and eccentric cylindrical collector systems, *Proc. ASME Solar Energy Div. Sixth Ann. Conf., Las Vegas*, pp. 194–200 (1984)
16 Lee, T. S. and Soh, C. L. Computational and experimental studies of convective heat transfer and fluid flow in eccentric annuli of rotating cylinders, *Proc. 3rd Australas. Conf. Heat Mass Transfer, Melbourne*, pp. 17–24 (1985)
17 Lee, T. S. Laminar fluid convection of varying Prandtl number in the annuli of rotating cylinders, *Proc. 9th Australas. Fluid Mech. Conf., Auckland*, pp. 90–92 (1986)
18 Lee, T. S. and Yeo, K. S. Laminar fluid convection of low Prandtl number fluid in the annuli of rotating cylinders, *Proc. 10th Australas. Fluid Mech. Conf., Melbourne*, Vol. 1, pp. 45–3.48 (1989)
19 Lee, T. S. Mixed convection of low Prandtl number fluids in the annuli of concentric rotating cylinders, *Thermophys. Heat Transfer*, **6**, 162–165 (1992)
20 Lee, T. S. Laminar fluid convection between eccentric heated horizontal rotating cylinders for low Prandtl number fluids, *Int. J. Num. Meth. Fluids*, **14**, 1037–1062 (1992)
21 Lee, T. S. Numerical computation of fluid convection with air enclosed between the annuli of eccentric heated horizontal rotating cylinders, *Comput. Fluids*, **21**, 355–368 (1992)
22 Ladeinde, F. Studies of thermal convection in self-gravitating and rotating horizontal cylinders in a vertical gravity field, *PhD Thesis*, Cornell University, Ithaca, NY (1988)
23 Prud'homme, M. and Robillard, L. Natural convection in an annular fluid layer rotating at weak angular velocity, *Proc. 4th Int. Symp. Transport Phenomena, Heat Mass Transfer, Sydney* (1991)
24 Yang, H. Q., Yang, K. T. and Lloyd, J. R. Natural convection suppression in horizontal annuli by azimuthal baffles, *Int. J. Heat Mass Transfer*, **31**, 2123–2135 (1988)
25 Yang, H. Q., Yang, K. T. and Lloyd, J. R. Rotational effects on natural convection in a horizontal cylinder, *AIChE J.*, **34**, 1627–1633 (1988)
26 Huetz, J. R. Natural and mixed convection in concentric annular spaces: experimental and theoretical results for liquid metal, *5th Int. Heat Transfer Conf., Tokyo*, **3**, 1364 (1974)
27 Gardiner, S. R. M. and Sabersky, R. H. Heat transfer in annular gap, *Int. J. Heat Mass Transfer*, **21**, 1459–1466 (1978)
28 Singh, M. and Rajvanshi, S. C. Heat transfer between eccentric rotating cylinders, *J. Heat Transfer*, **102**, 347–205 (1980)
29 Fuseki, T., Farouk, B. and Ball, K. S. Mixed-convection flows within a horizontal concentric annulus with a heated rotating inner cylinder, *Num. Heat Transfer*, **9**, 591–604 (1986)
30 Ratzel, A. C., Hickox, C. E. and Gartling, D. K. Technique of reducing thermal conduction and natural convection heat losses in annular receiver geometries, *J. Heat Transfer*, **101**, 108–113 (1979)
31 Projahn, U, Reiger, H. and Beer, H. Numerical analysis of laminar natural convection between concentric and eccentric cylinders, *J. Num. Heat Transfer*, **4**, 131–146 (1981)
32 Roache, P. J. *Computational Fluid Dynamics*, Hermosa, Albuquerque, NM (1973)
33 Peaceman, D. W. and Rachford, H. H. Numerical solution of parabolic and elliptic differential equations, *J. Soc. Indust. Appl. Math.* **3** (1), 28–41 (1955)
34 McKees, S. and Michell, A. R. Alternating direction methods for parabolic equations in two space dimensions with mixed derivatives, *The Comput. J.*, **13**, 81–86 (1970)
35 Grigull, U. and Hauf, W. (1966) Natural convection in horizontal cylindrical annuli, *3rd Int. Heat Transfer Conf., Chicago*, pp. 182–195 (1966)
36 Raithby, G. D. and Hollands, K. G. T. A general approximation solutions to laminar and turbulent convection problems, *Adv. Heat Transfer*, **11**, 265–315 (1975)